Mechanism for Unimolecular Decomposition of HMX (1,3,5,7-Tetranitro-1,3,5,7-tetrazocine), an ab Initio Study

Debashis Chakraborty, Richard P. Muller, Siddharth Dasgupta, and William A. Goddard III*

Materials and Process Simulation Center (MSC), Beckman Institute (139-74), Division of Chemistry and Chemical Engineering, California Institute of Technology, Pasadena, California 91125

Received: July 24, 2000; In Final Form: November 17, 2000

To improve the mechanistic understanding of the possible decomposition in the gas phase of the energetic material HMX (octahydro-1,3,5,7-tetranitro-1,3,5,7-tetrazocine), we used ab initio calculations to determine the various unimolecular decomposition channels. We find three distinct mechanisms: (i) homolytic cleavage of N−N bond to form NO_2 ($M = 46$) and HMR ($M = 250$) which subsequently decomposes to form various products; (ii) successive HONO eliminations to give four HONO ($M = 47$) plus a stable intermediate ($M = 108$); (iii) O-migration from one of the NO_2 groups of HMX to neighboring C atom followed by the decomposition of intermediate ($M = 296$) to INT222 (a ring-opened RDX structure) and MN-oring ($M = 74$), which can undergo dissociation to smaller mass fragments. The decomposition scheme for HMX is similar to that for RDX presented earlier (*J. Phys. Chem. A* **2000**, *104*, 2261), except that concerted decomposition of HMX to four MN ($M = 74$) molecules is not a favorable decomposition pathway, whereas this pathway was found in RDX decomposition (both experimentally and theoretically). The formation of RDR-o in the N−N homolysis pathway 1 or the formation of INT222 in pathways 1 and 3 presents an unified mechanistic scheme for the decomposition of both of these nitramines. The HMX decomposition mechanism correlates with available condensed phase experimental results, but detailed comparison of the predicted gas phase energetics is not possible.

1. Introduction

The cyclic nitramines, octahydro-1,3,5,7-tetranitro-1,3,5,7-tetrazocine (HMX), and hexhydro-1,3,5-trinitro-1,3,5-triazine (RDX), are important energetic materials with applications ranging from explosives and rocket propellants to automobile air bags. They release large amounts of energy through a bulk decomposition process, which is very complicated involving both unimolecular and bimolecular reactions. Understanding the underlying complex chemical processes is essential to obtain to an improved model for combustion or detonation of these energetic materials.

Unlike RDX, where Zhao et al.[1] studied the gas phase decomposition using IRMPD technique, experimental studies of HMX are limited to condensed phase decomposition.[2−17] Reported decomposition products vary greatly depending on such experimental conditions as heating rate, sample dimensions, and the composition of the surrounding matrix. This has made unambiguous identification of the primary decomposition products difficult. However, most experiments agree that the final gas phase products from the burning surface are smaller mass fragments such as NO_2, N_2O, NO, CH_2O, CO, N_2, HCN, H_2O, H_2, and CO_2. In order to determine the initial steps, we focus on the gas phase unimolecular decomposition mechanism of HMX.

2. Current Work

In this paper we present a comprehensive mechanistic study of the thermal decomposition of HMX based on ab initio quantum mechanics, using density functional methodology (DFT-B3LYP). This is a continuation of our previous work[18] on RDX, using exactly the same methods. Section 3 surveys the experimental and theoretical work in the published literature, section 4 outlines the computational methods, and section 5 presents the results. These are compared to experiments in section 6 with concluding remarks in section 7.

3. Literature Survey

3.1. Experimental Studies. Suryanarayana et al.[2a] studied thermal decomposition of HMX at $T = 230$, 254, and 280 °C using mass spectrometry. They proposed a concerted decomposition mechanism of HMX to four methylenenitramine (MN) molecules, which can further decompose to CH_2O and N_2O. In a separate experiment using ion impact fragmentation of HMX, Suryanarayana et al.[2b] detected mass fragments of 30, 46, 75, 120, 128, 148, 205, and 222 in the mass spectra.

Goshgarian[3] detected large molecular masses with $m/e = 222$, 175, 148, 128, 120, and 81 in addition to the usual smaller mass fragments in the thermal decomposition of HMX in an on-stream reactor at 240−290 °C. The mass peak at 222 was attributed to a ring open RDX structure, which can subsequently decompose to 175, 148, 128, etc.

Farber and Srivastava[4] detected several decomposition products at $m/e = 222$, 148, 128, 120, 102, 74, 56, 46, 32, 30, 28, and 18. 148 was the major decomposition product of HMX at 175−275 °C. They proposed a homolytic cleavage of the HMX ring to two 148 ($C_2H_4N_4O_4$) fragments which can form two MN molecules via subsequent decomposition. They also detected peaks at $m/e = 249$ and 250 as a result of the elimination of HNO_2 and NO_2 from HMX. Moreover, the $m/e = 120$ was attributed to reactions of gaseous products with the condensed phase.

Morgan and Bayer[5] in their pyrolysis study using electron spin resonance (ESR) detected CH_2N and NO_2 radicals as the decomposition products coming from MN intermediates.

In contrast, decomposition of HMX in solution[6] does not yield any gaseous NO or NO_2 radicals.

10.1021/jp0026181 CCC: $20.00
Published on Web 02/03/2001

From high-temperature pyrolysis studies[7−9] several plausible schemes were proposed involving the formation of $m/e = 222$, 176, 175, 148, 128, 102, 81, etc. These larger molecular masses can further dissociate to the observed smaller gaseous products.

Using simultaneous thermogravimetric modulated beam mass spectrometry and isotope scrambling experiments, Behrens and Bulusu[10] and Behrens[11,12] observed gaseous pyrolysis products such as H_2O, HCN, CO, CH_2O, NO, N_2O, CH_3NHCHO, $(CH_3)_2$-NNO, 1-nitroso-3,5,7-trinitro-1,3,5,7-tetrazocine (ONTNTA), and a nonvolatile polyamide residue between 210 and 235 °C. They suggested several different reaction branches to understand the complex decomposition process of HMX in condensed phase. Their results also support the water-catalyzed decomposition of HMX where water is trapped within HMX particles.[8,9,13]

In the recent CO_2 laser assisted combustion of HMX, Tang et al.[14,15] detected several larger molecular masses at 97, 81, 70, 54, 47, 45, 43, and 42 as minor species in addition to the usual small mass fragments in the HMX flame structure.[16]

Brill[17] suggested two competing global reactions during the thermal decomposition of condensed phase HMX:

$$\mathrm{HMX} \rightarrow 4(\mathrm{HONO} + \mathrm{HCN})$$

$$\mathrm{HMX} \rightarrow 4(\mathrm{CH_2O} + \mathrm{N_2O})$$

However, in laser-assisted self-oscillating burning of HMX, Tang et al.[15] concluded that a multiple step reaction at condensed phase might explain the experimental data more realistically.

Summarizing the wide array of condensed phase experimental observations, there is agreement in identifying the major gaseous products in the HMX flame structure. However, several plausible mechanistic schemes have been proposed for the condensed phase decomposition of HMX. Most experimental studies support the formation of CH_2O, N_2O, HONO, and HCN as the condensed phase decomposition products, which further decompose to the gaseous products in the HMX flame.

3.2. Theoretical Studies. Very few theoretical studies have previously been reported for HMX. A conformational study based on quantum chemistry (DFT at the B3LYP level) was used to derive a force field.[19] Using the force field the effect of hydrostatic pressure on the packing of HMX crystal[20,21] was studied with molecular dynamics simulations. A quantum mechanics calculation (DFT at the B3LYP level) of the electronic structure was used to predict the nuclear quadrupole interactions in HMX.[22]

Melius and Binkley[23] used empirically corrected ab initio quantum mechanics (BAC-MP4) on nitramine-containing systems to estimate the energetics of the reactants, products, and possible intermediates for RDX and HMX, suggesting some possible decomposition mechanisms. Their studies also included the possibility of water-catalyzed decomposition of HMX.

4. Computational Methods

We optimized the geometries of the reactants, products, intermediates, and transition states (TS) at the B3LYP flavor of density functional theory. This includes the generalized gradient approximation (Becke 1988 non local gradient correction), exact exchange using the Becke three-parameter exchange functional,[24] and the nonlocal correlation functional of Lee, Yang, and Parr.[25] We used the 6-31G(d) basis set, which is consistent with our earlier investigations on RDX. This level of theory is expected to predict the energetics of large molecular systems like RDX to within a few kcal/mol.[26,27]

All stationary points have been positively identified as local minima [all curvatures positive from diagonalizing the Hessian, (NIMAG) = 0] or as transition states TS [exactly one negative curvature, NIMAG = 1]. Vibrational frequencies were calculated at all stationary points to obtain zero point energies (ZPE) and thermodynamic parameters (entropy and enthalpy as a function of temperature). All calculations were carried out with Jaguar quantum chemistry program package.[28]

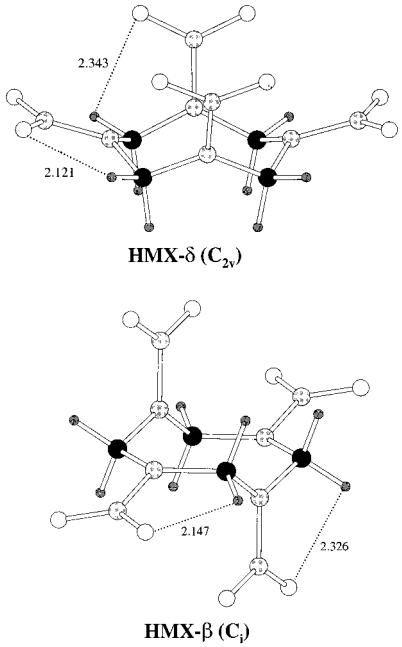

Figure 1. Optimized geometries of HMX in δ and β form.

5. Results

Figure 1 shows the optimized geometry of HMX for delta (a boatlike conformation) and beta (a chairlike conformation). The optimized structures of the decomposition products are shown in Figure 2 while the various TS are presented in Figure 3. Table 1 gives the relative energies of two possible initial decomposition processes:

(i) N−N homolysis and

(ii) HONO elimination.

The vibrational frequencies of all the stable intermediates and some important products are given in Table 2 while the frequencies for all the TS are given in Table 3.

The potential energy profile of the unimolecular decomposition mechanism is illustrated in Figures 4, 5, and 6. These various results for HMX and the analogous results for RDX[18] are combined into a generalized decomposition scheme for RDX and HMX in Figure 7.

The optimized geometries (*XYZ* coordinates) of all the reactants, products, intermediates, and TS are included as supplementary information (Tables S1−S12).

Here and in the Discussion, the energies are corrected for ZPE. Where this correction is *not* made, we will indicate so by adding "no ZPE".

5.1. Conformations of HMX. Crystalline HMX can exist in four polymorphic phases: α, β, γ, and δ. The β form, stable at room temperature, has a monoclinic structure with two chairlike molecules of C_i symmetry per unit cell.[29] The δ HMX crystal, stable in the temperature range 103−162 °C, has C_2 symmetry and crystallizes in orthorhombic symmetry with eight boatlike molecules per unit cell.[30] The molecular structures of the α and γ forms of HMX are quite similar to that of δ form, but the precise 2-fold symmetry axis of δ is missing.[31,32] In addition, the γ form is a hydrate.

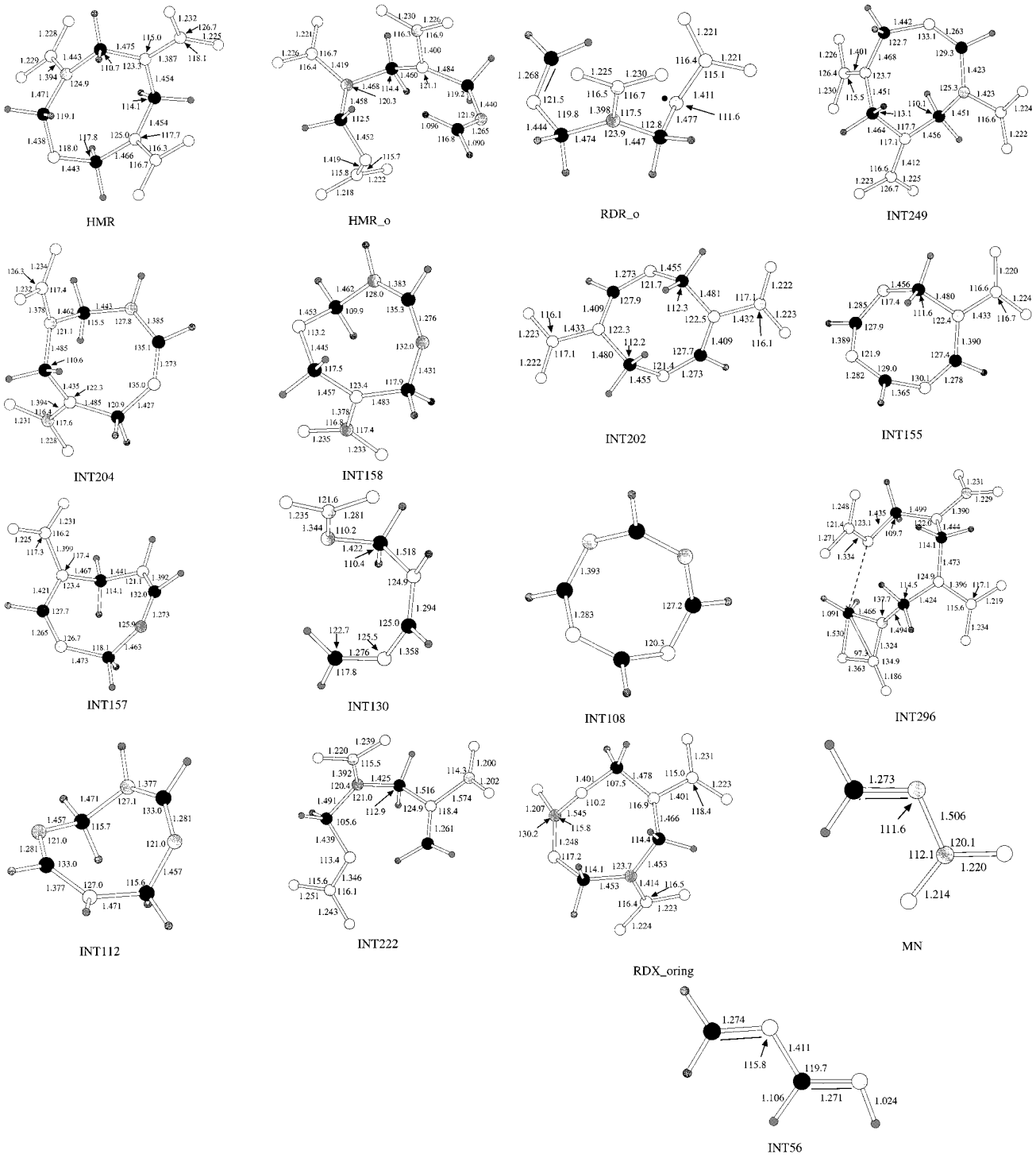

Figure 2. Optimized structures of the intermediates and some important products in the unimolecular decomposition of HMX. The large solid, dark gray, and light gray circles represent the C, N, and O, respectively, and the small gray circle represents H atoms.

Thus, considering the various polymorphic forms of HMX, we find two primary molecular conformations, chair (β) and boat (δ), as shown in Figure 1. The β form is 2.5 kcal/mol *more* stable than the δ form (2.0 kcal/mol including ZPE) at the B3LYP/6-31G(d) level of theory. This compares well with the energy differences of 2.1 kcal/mol predicted at the B3LYP/6-311G(d,p) level, 3.5 ± 1.0 kcal/mol at the B3LYP/6-311G(d,p)//MP2/6-311G(d,p) level. Indeed using the classical force field,[19] the energy difference is 2.6 kcal/mol.

It is conceivable that flexible cyclic nitramines like HMX might exhibit some additional metastable nonsymmetric low-energy conformations, besides the chair and boat forms. However, such low-energy conformers would have little impact on the mechanism of thermal decomposition. In this work, we perform all our calculations on the β conformation, the most stable form and the one exhibited in the crystal at room temperature.

5.2. Initiation of Decomposition. Three distinct initial decomposition channels have been identified for RDX in our earlier study:[23]

(1) concerted ring breaking,

(2) homolysis of $N-NO_2$ bond, and

(3) HONO elimination.

Since the molecular structure of HMX has NO_2 groups with two different orientations (two equatorial and two axial, see

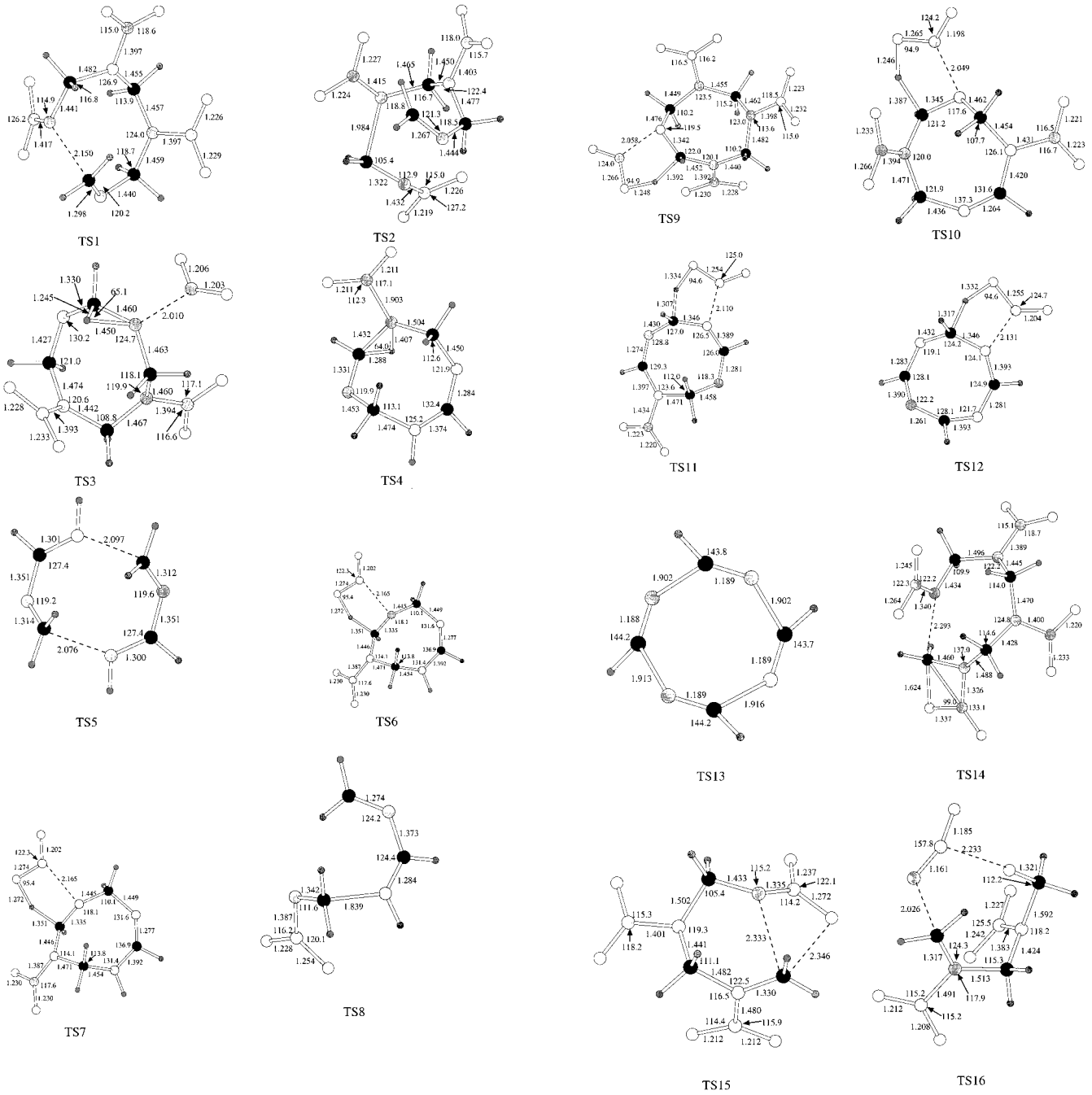

Figure 3. Optimized structures of the transition states in the unimolecular decomposition of HMX. Symbols stand for C, N, O and H atoms, respectively, as described in Figure 2.

TABLE 1: Relative Energies[a] for Two Competitive Initial Decomposition Processes in HMX

	β-HMX	δ-HMX
$N-NO_2$ bond cleavage		
eq HMR radical	43.6	45.6
ax HMR radical	46.5	45.4
HONO elimination TS	49.0	50.6

[a] Without ZPE correction.

Figure 1), it is likely that there will be preferential elimination of one NO_2 group over the other. We explored these possibilities, with the results summarized in Table 1.

The concerted ring scission involves breaking alternate C−N bonds and multiple possibilities do not exist.

Table 1 clearly shows that removal of NO_2 from equatorial position generates the most stable $C_4H_8N_7O_6$ (HMR) radical. 43.6 kcal/mol energy is required to remove one equatorial NO_2 whereas 46.5 kcal/mol is required for removing the axial NO_2 from β HMX. In δ HMX, dissociation energy of both sets of $N-NO_2$ bonds are roughly equal. Thus, in β HMX the N−N homolytic pathway can initiate by the preferential elimination of an equatorial NO_2 group.

The concerted HONO elimination involves breaking of both $N-NO_2$ and C−H bonds. The short nonbonded N−O:::H−C distance plays an important role in HONO elimination. The N−O:::H−C distance is smaller for equatorial NO_2 groups in both β and δ HMX as shown in Figure 1. Because of weak equatorial NO_2 bond and closer nonbonded O:::H distance, the concerted HONO elimination will preferentially occur from

TABLE 2: Calculated Frequencies of the Intermediates and Some Important Products at the B3LYP/6-31G(d) Level of Theory[a]

HMR														
40	62	68	74	101	104	117	129	168	226	246	289	339	371	384
398	413	433	525	600	628	636	652	702	751	758	763	769	845	852
859	897	922	944	962	964	1069	1129	1154	1183	1230	1233	1262	1317	1321
1342	1343	1354	1361	1387	1403	1424	1431	1444	1467	1473	1506	1509	1662	1668
1674	3040	3047	3105	3110	3130	3157	3177	3190						
HMR-o														
22	32	53	60	75	98	103	111	133	151	194	210	256	278	330
335	391	403	460	471	505	584	611	622	672	681	727	751	770	803
852	857	871	928	977	982	996	1057	1064	1073	1159	1188	1222	1236	1271
1317	1338	1366	1372	1390	1398	1417	1453	1473	1487	1515	1521	1658	1670	1690
1779	3071	3074	3092	3132	3132	3142	3186	3193						
INT204														
45	66	86	100	126	154	184	227	317	340	384	403	416	475	483
523	597	629	677	712	751	755	767	848	864	913	930	954	955	1016
1031	1153	1155	1205	1239	1241	1315	1317	1349	1363	1377	1396	1426	1445	1479
1492	1498	1500	1532	1639	1655	1795	3038	3082	3101	3139	3144	3161	3190	3580
INT158														
43	77	111	124	190	256	332	338	386	457	489	536	540	634	702
751	772	849	876	892	905	950	995	1025	1099	1124	1146	1199	1228	1287
1301	1323	1345	1375	1394	1426	1449	1485	1514	1516	1531	1627	1766	3013	3041
3061	3097	3108	3110	3126	3571									
INT157														
59	100	126	177	214	249	342	404	459	492	529	578	604	647	747
751	801	855	886	920	938	952	983	1001	1075	1150	1199	1238	1261	1326
1357	1395	1411	1428	1459	1491	1517	1552	1664	1731	1763	2986	3093	3108	3137
3188	3195	3554												
INT130														
56	118	147	171	222	249	382	416	499	564	646	697	731	789	805
816	943	993	1060	1113	1120	1165	1225	1258	1284	1333	1384	1473	1489	1532
1555	1677	1751	3054	3068	3134	3172	3196	3482						
INT112														
88	209	249	270	358	430	511	530	599	612	767	825	896	905	950
977	979	996	1073	1154	1201	1233	1284	1307	1376	1407	1454	1460	1513	1519
1536	1566	1713	1753	3040	3069	3089	3101	3102	3105	3575	3578			
INT222														
18	36	49	74	99	112	115	186	199	249	270	308	340	362	387
428	508	560	608	640	647	717	747	763	771	775	809	823	879	945
1000	1063	1128	1160	1175	1197	1250	1268	1277	1305	1323	1355	1374	1381	1409
1461	1528	1551	1627	1655	1807	2390	3041	3090	3130	3205	3211			
RDR-o														
51	64	69	78	94	115	182	222	258	345	397	444	463	506	597
607	675	697	758	780	849	853	942	956	989	1000	1079	1156	1212	1220
1304	1332	1353	1368	1387	1417	1462	1488	1519	1634	1658	1758	3070	3077	3087
3131	3149	3170												
INT249														
34	66	80	86	104	108	117	190	253	267	307	320	339	369	401
433	455	497	546	571	590	629	662	675	711	748	757	788	820	845
888	898	929	955	996	1030	1121	1164	1199	1244	1249	1295	1311	1333	1394
1481	1493	1547	1558	1597	1634	1653	1669	1706	1723	1834	1891	1907	1916	3052
3061	3066	3130	3138	3148	3157									
INT202														
44	60	81	95	174	208	236	247	332	343	422	451	467	494	529
537	619	639	741	741	787	795	858	859	917	929	969	971	1001	1009
1104	1162	1229	1245	1292	1309	1312	1331	1399	1401	1428	1443	1527	1561	1685
1694	1720	1731	3047	3077	3172	3175	3210	3213						
INT155														
64	78	175	237	244	304	349	429	461	487	546	652	676	740	771
806	871	922	957	965	980	1007	1043	1111	1139	1255	1316	1324	1397	1402
1426	1445	1520	1641	1685	1697	1739	3048	3138	3141	3189	3224			
INT108														
229	231	302	320	433	437	704	715	715	864	960	981	984	1015	1034
1060	1061	1114	1387	1407	1409	1430	1632	1686	1697	1698	3143	3145	3146	3148
INT296														
38	56	71	90	98	103	113	128	133	150	162	190	204	226	269
339	348	370	376	405	429	472	559	594	629	638	649	664	690	703
711	751	753	758	799	832	867	880	932	934	947	1047	1052	1085	1099
1114	1123	1170	1207	1218	1222	1283	1293	1303	1314	1336	1355	1390	1400	1411
1437	1447	1474	1478	1497	1511	1525	1649	1680	1807	3073	3085	3101	3116	3129
3148	3184	3273												

TABLE 2 (Continued)

RDX-o ring														
48	73	82	100	116	181	194	227	257	303	359	410	420	437	465
492	576	585	620	646	693	724	748	754	761	842	872	917	936	996
1041	1073	1104	1185	1202	1253	1271	1305	1328	1338	1355	1388	1397	1422	1443
1464	1489	1517	1663	1689	1757	3063	3087	3117	3145	3196	3197			
MN														
34	398	523	553	633	828	870	1080	1181	1349	1424	1683	1718	3126	3236
INT56														
123	378	627	633	911	979	1068	1087	1208	1301	1437	1505	1700	1728	2950
3004	3167	3436												

[a] All frequencies are in cm^{-1}.

TABLE 3: Calculated Frequencies of the Transition States at the B3LYP/6-31G(d) Level of Theory[a]

TS1														
-424	39	61	66	76	98	104	134	136	166	209	241	264	300	344
360	381	414	447	505	585	600	613	627	692	733	749	754	770	810
825	857	871	918	935	951	1007	1044	1056	1104	1167	1187	1204	1252	1271
1292	1310	1330	1350	1379	1383	1394	1420	1441	1467	1482	1496	1570	1622	1653
1668	3048	3055	3066	3106	3116	3127	3176	3221						
TS2														
−546	22	36	55	60	73	76	100	117	123	151	188	197	223	289
315	346	373	413	428	510	547	577	593	606	638	681	696	753	782
793	844	848	853	929	955	964	995	1002	1071	1101	1148	1180	1206	1221
1301	1303	1330	1342	1349	1370	1395	1436	1458	1477	1511	1526	1626	1642	1656
1758	3054	3069	3081	3132	3135	3137	3167	3255						
TS3														
−2008	18	43	61	77	93	96	115	141	160	174	232	243	284	287
364	379	401	417	455	479	514	581	635	677	696	734	743	752	755
776	850	859	895	937	943	960	972	1082	1096	1181	1197	1219	1234	1306
1322	1331	1353	1363	1379	1386	1415	1432	1458	1461	1478	1510	1520	1643	1654
1735	2054	3030	3070	3105	3112	3136	3141	3176						
TS4														
−2004	47	55	125	151	195	228	264	295	324	359	477	496	550	567
618	730	764	802	817	850	905	950	978	995	1078	1136	1150	1194	1208
1257	1283	1347	1362	1396	1416	1456	1466	1513	1533	1571	1703	1712	1871	3040
3077	3114	3118	3130	3137	3567									
TS5														
−357	79	144	172	213	247	302	362	428	475	665	731	775	783	916
958	1021	1024	1062	1069	1119	1144	1211	1215	1289	1295	1425	1430	1474	1483
1529	1590	1620	1667	3066	3067	3084	3089	3185	3190	3476	3479			
TS6														
−1535	59	76	94	110	127	153	190	194	277	340	358	367	404	411
465	477	521	555	578	655	721	752	769	808	872	875	943	956	1003
1024	1038	1098	1153	1207	1240	1253	1271	1298	1327	1354	1360	1378	1420	1477
1489	1496	1518	1528	1564	1652	1756	1773	2989	3015	3094	3101	3125	3196	3595
TS7														
−321	72	84	110	143	176	196	204	241	292	377	412	469	483	627
673	685	754	784	805	880	890	926	984	1036	1079	1106	1144	1186	1212
1287	1322	1350	1413	1471	1485	1529	1558	1613	1799	1988	3063	3110	3128	3134
3234	3307	3583												
TS8														
−276	52	87	111	152	184	212	372	420	483	540	648	701	784	800
810	920	1011	1031	1060	1115	1204	1216	1229	1282	1321	1335	1430	1511	1530
1606	1679	1751	3080	3107	3118	3190	3205	3539						
TS9														
−1567	35	61	73	77	89	93	113	117	125	166	176	205	234	250
275	320	370	380	396	424	462	468	522	553	586	608	627	663	691
725	740	749	752	758	797	835	872	883	921	932	958	968	1000	1065
1150	1193	1205	1223	1259	1271	1292	1305	1325	1335	1344	1349	1375	1383	1392
1423	1438	1461	1475	1503	1514	1599	1652	1663	1689	1833	3085	3096	3104	3109
3162	3181	3189												
TS10														
−1590	57	70	77	83	91	98	117	189	203	233	247	285	330	362
397	454	472	484	508	531	552	575	671	685	728	745	751	767	801
868	889	901	926	955	976	990	1009	1129	1150	1220	1251	1269	1298	1319
1332	1352	1360	1391	1404	1431	1452	1472	1481	1521	1612	1661	1705	1800	1850
3071	3118	3120	3172	3208	3217									

TABLE 3 (Continued)

TS11														
−1436	38	68	96	118	144	168	205	237	303	323	395	420	458	486
511	524	576	659	669	739	772	789	805	875	907	944	966	987	999
1020	1061	1139	1245	1266	1317	1325	1337	1344	1399	1402	1445	1481	1525	1593
1663	1697	1728	1770	3060	3066	3167	3192	3218						
TS12														
−1441	84	119	160	202	236	285	315	351	410	484	502	567	680	728
735	799	846	957	964	995	1002	1014	1026	1044	1097	1237	1328	1332	1392
1410	1423	1481	1571	1645	1687	1695	1764	3057	3137	3143	3181			
TS13														
−740	94	100	134	156	158	164	183	192	291	517	523	525	576	794
802	807	813	1041	1103	1109	1124	1817	1991	1994	2035	3298	3300	3304	3306
TS14														
−251	38	61	73	90	98	110	115	129	148	160	191	195	239	241
288	358	365	379	389	414	436	474	594	595	636	648	660	698	705
719	751	753	760	795	831	861	878	933	933	943	1043	1052	1092	1102
1114	1132	1180	1211	1221	1225	1285	1295	1301	1314	1337	1357	1389	1398	1410
1436	1443	1456	1478	1499	1509	1537	1650	1681	1786	3074	3095	3104	3124	3157
3165	3186	3305												
TS15														
−379	46	65	69	81	108	127	196	239	267	325	341	364	397	433
443	566	586	609	658	687	709	752	757	765	784	830	839	918	932
944	990	1070	1127	1173	1210	1224	1264	1297	1314	1331	1346	1371	1416	1431
1475	1506	1530	1535	1665	1756	3033	3071	3136	3204	3246	3362			
TS16														
−333	46	58	66	83	99	109	143	182	227	237	289	318	334	374
397	427	453	536	564	576	598	625	682	727	761	772	816	849	910
973	1035	1081	1125	1205	1257	1260	1303	1307	1328	1342	1352	1376	1411	1427
1475	1536	1549	1630	1763	2151	2910	3017	3022	3125	3196	3275			

[a] All frequencies are in cm^{-1}, and the negative numbers indicate imaginary frequencies.

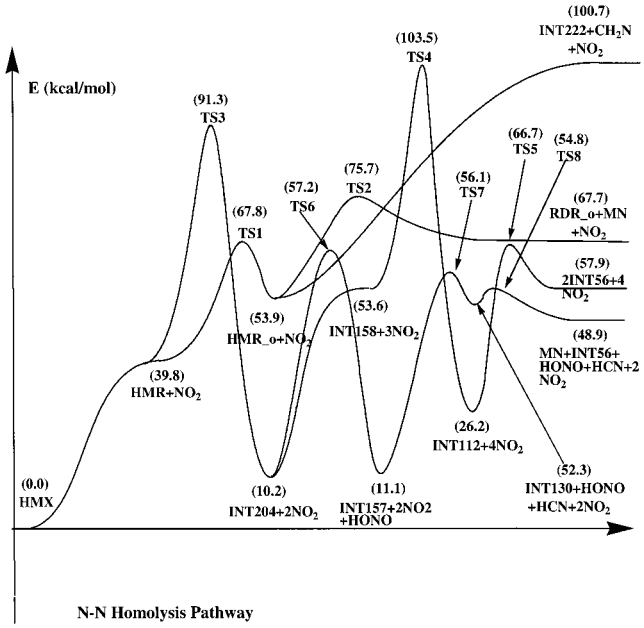

Figure 4. Potential energy profile for N−N homolysis from HMX and further decomposition of the intermediate radicals.

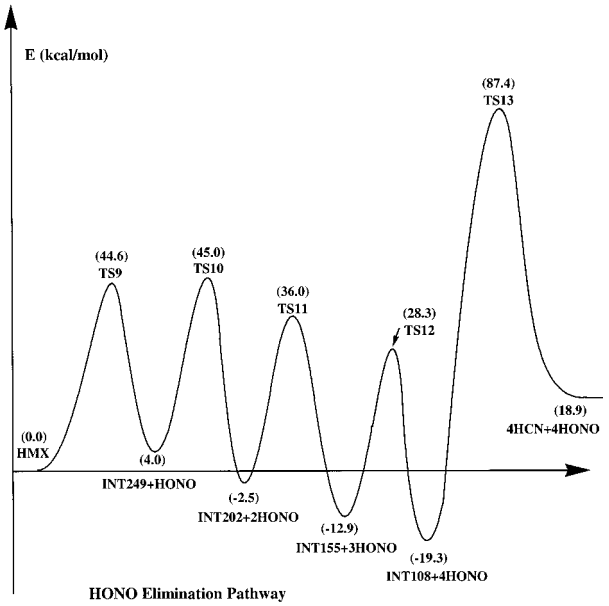

Figure 5. Potential energy profile for HONO elimination from HMX and following decompositions.

equatorial NO_2. The HONO elimination from δ HMX is 1.6 kcal/mol higher than from β HMX.

5.3. Reaction Path 1. Homolytic N−N Bond Fission plus Subsequent Decomposition. *5.3.1. N−NO_2 Homolysis To Form HMR.* N−NO_2 bond breaking is most likely a barrierless low-energy decomposition pathway for both RDX and HMX. As discussed above, elimination of NO_2 will occur preferentially from the equatorial position. We calculate a N−N bond dissociation energy of 39.8 kcal/mol (including ZPE) for HMX. This is in very good agreement with our earlier calculated N−N bond dissociation energy of 39.0 kcal/mol for RDX.[18]

In their BAC-MP4 study, Melius and Binkley estimated a dissociation energy of ∼48 kcal/mol for the N−NO_2 bond.[23] Their estimation was based on the assumption that the N−N bond strength in RDX and HMX should be very similar to that of some smaller nitramines, such as methylenenitramine. However, the N−N bond in both RDX and HMX is somewhat weaker than that of some related nitramines.[27] The estimated N−N bond dissociation energies [at the B3LYP/6-311G(d,p)//B3LYP/6-31G(d) level with scaled HF/6-31G(d) ZPE correction] in related nitramines are 46 (dimethylnitramine), 48 (1-nitropiperidine), and 49 (1-nitro-1,3,5-triazine), where in each

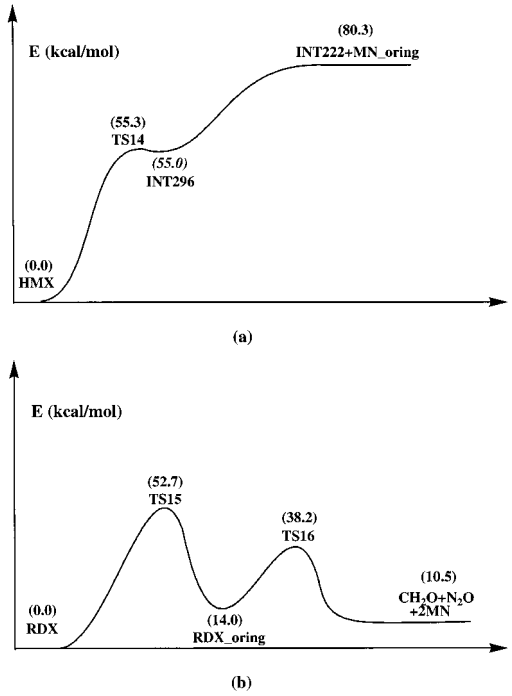

Figure 6. (a) Potential energy profile of the O-migration pathway of HMX leading to the formation of INT222 and MN-oring. (b) Potential energy profile of the O-migration pathway of RDX.

case 6 kcal/mol was added to correct the energy for expected error.[27] The N−N bond strength in RDX is 42.0 kcal/mol (with 6 kcal/mol error correction) at the same level of theory.[27] In contrast, the N−N bond in MN (35.9 kcal/mol (including ZPE) at the G2M level of theory)[33] is weaker than these nitramines.

5.3.2. Subsequent Decomposition of HMR. Following our earlier RDX study, we calculated two main pathways for HMR decomposition, shown in Figure 4:

(i) ring opening pathway and

(ii) successive NO_2 elimination.

Although it is a relatively high-energy pathway, (2) is included to explain some of the observed mass fragments. The ring opening of HMR and subsequent decomposition was also proposed by Melius and Binkley as one of the important degradation pathways of RDX and HMX.[23]

5.3.3. Ring-Opening Pathway for HMR Decomposition. 5.3.3.1. Formation of HMR-o + NO_2. The lowest energy decomposition pathway of HMR is the opening of the radical ring. This requires an additional 28.0 kcal/mol. The ring-opened structure (HMR-o) is 14.1 kcal/mol less stable than HMR.

The ring opening of HMR occurs through the breaking of the C−N bond between the C atom adjacent to the radical center and the nitrogen atom next to it. TS1 was generated by first scanning the dissociating C−N bond from 1.5 to 2.4 Å at 0.1 Å interval to find a candidate TS. Each point along the reaction coordinate was then optimized fully (except the reaction coordinate). The maximum, centered at 2.1 Å, was then fully optimized (requiring a single negative curvature) to locate saddle point TS1. The breaking CN bond in TS1 is 2.15 Å. To locate the minimum energy structure of HMR-o, we started with the optimized structure at 2.4 Å from the scan and optimized it fully leading to HMR-o. This confirms that TS1 properly connects HMR and HMR-o. HMR-o is the ring open structure of HMR as shown in Figure 2. The terminal CH_2N group has a CN double bond length of 1.265 Å (compare to similar CN π bond in MN, 1.274 Å) and the radical is centered on the ring opened N-atom. The broken CN bond distance is 3.522 Å in HMR-o.

5.3.3.2. Decomposition of HMR-o. In RDX, the lowest energy decomposition pathway from RDR-o was found to form INT176 via a hydrogen atom migration.[18] We did not find such a hydrogen migration in the decomposition of HMR-o. Larger nonbonded contact between H-atom of the ring-opening CH_2 group and the N radical is not favorable for such migration in HMR-o. Instead, we find two distinct decomposition pathways via the elimination of CH_2N and MN from HMR-o.

Elimination of MN molecule from HMR-o leads to the formation of RDR-o (m/e = 176) via TS2. TS2 has a barrier of 21.8 kcal/mol with respect to HMR-o. TS2 was also located by scanning the breaking CN bond of HMR-o. TS2 properly connects HMR-o with RDR-o + MN. RDR-o, also formed in

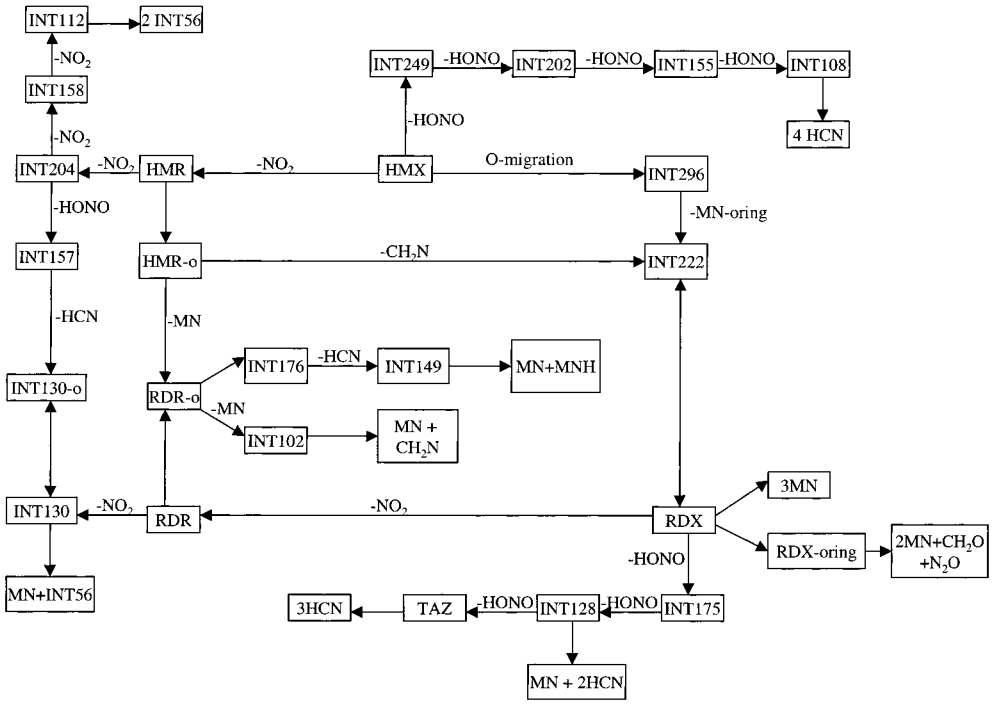

Figure 7. A unified decomposition scheme for RDX and HMX.

the decomposition of RDX, is the ring-opened structure of RDX radical (RDR).[18] Possible decomposition of RDR-o to various smaller mass fragments was discussed in detail in our earlier RDX study.[18]

Alternatively, HMR-o can eliminate one CH_2N radical to form INT222 + CH_2N. We scanned the reaction path of CH_2N elimination and did not find any appreciable barrier. Since the elimination of CH_2N proceeds via a simple homolytic cleavage of the C−N bond and does not involve any intramolecular rearrangement, absence of reaction barrier is understandable. INT222 has the same molecular weight and stoichiometry of RDX. It is actually a ring-opened biradical structure of RDX resulting from the rupture of one of the ring CN bonds.

INT222 is 56.0 kcal/mol higher in energy than RDX. Formation of INT222 from RDX thus occurs through a barrierless dissociation of one of the ring C−N bonds. C−N bond energies of some related compounds like nitromethane and dimethylnitramine at similar B3LYP level of theory with variety of basis sets range between 52 and 55 kcal/mol.[34] The simultaneous breaking of three CN bonds in RDX, leading to the formation of three MN molecules, required ∼59.4 kcal/mol at the same level of theory.[18] INT222 + CH_2N is 100.7 kcal/mol more endothermic than HMX. Further decomposition of INT222 to three MN molecules would require even higher energy. On the other hand, it could recombine back to RDX, which can undergo further dissociations.

Formation of RDR-o and INT222 in the thermal decomposition of HMX makes the connection between HMX and RDX decomposition mechanisms and supports the observed similarity in their experimental spectra. This will be discussed in more detail in the discussion section.

5.3.4. Subsequent NO_2 Elimination from HMR. 5.3.4.1. Elimination of second NO_2. The elimination of a second NO_2 group from HMR becomes difficult due to formation of a biradical (unpaired spin on each of the two N radical centers). This high-energy conformation can be avoided by H-migration with simultaneous NO_2 elimination. This leads to TS3, as shown in Figure 4. As the N−NO_2 distance increases in TS3, the H atom from the neighboring CH_2 group migrates to the N-atom and the adjacent C−N bond (between the N radical in HMR and H migrating C) gains partial double bond character (1.330 Å). The breaking N−N bond in TS3 is 2.010 Å and the migrating H atom is 1.450 and 1.245 Å away from the N and C atoms, respectively. TS3 has a barrier of 51.5 kcal/mol over HMR and goes to INT204. Since TS3 involves a hydrogen migration, it has a large negative eigenvalue of 2008 cm^{-1}. INT204 is a relatively stable intermediate with only 10.2 kcal/mol endothermicity over HMX.

5.3.4.2. Elimination of Third NO_2. The third NO_2 elimination from INT204 involving N−NO_2 homolytic cleavage requires an additional 43.4 kcal/mol. Thus the formation of radical intermediate INT158 does not have any appreciable reaction barrier similar to the formation of HMR from HMX.

5.3.4.3. Elimination of Fourth NO_2. INT158 can further undergo NO_2 elimination in a way similar to the second NO_2 elimination from HMR. The transition structure TS4 involves simultaneous NO_2 elimination and H migration to avoid the formation of the high-energy biradical species. TS4 has a barrier of 49.9 kcal/mol over radical intermediate INT158 and properly connects INT158 with INT112. Elimination of NO_2 and subsequent H migration to the N-atom allows π bonding between N-radical and H migrating C. This in turn brings planarity to the ring. Intermediate INT112 has both the C−N π bonds at ∼1.28 Å.

5.3.4.4. Concerted Breaking of INT112. INT112 can further decompose in a concerted way to two CH_2NCHNH (INT56, M = 56) via TS5. The breaking CN bonds in TS5 are 2.076 and 2.097 Å, respectively. The degradation product INT56 has a planar structure and was also found in the subsequent NO_2 elimination pathway of RDX.[18]

5.3.4.5. HONO Elimination from INT204. Instead of eliminating the third NO_2, an alternate pathway for the decomposition of INT204 might be HONO elimination and subsequent decomposition. We looked for an alternative low-energy pathway of formation of INT56. The HONO elimination preferentially takes place via the elimination of CH_2 hydrogen next to NH in INT204 and neighboring NO_2 group. The breaking N−N bond in TS6 is 2.165 Å apart and the migrating H atom is 1.351 and 1.272 Å away from C and O atom. Formation of CN π bond brings more planarity to INT157. TS6 has a barrier of 47.0 kcal/mol over INT204. Thus the barrier for HONO elimination is higher than the third NO_2 elimination from INT204. But the associated lower endothermicity in the subsequent decomposition makes the latter pathway more favorable.

5.3.4.6. Decomposition of INT157 to MN + INT56 + HCN. INT157, which is 11.1 kcal/mol less stable than HMX, can further dissociate to MN + INT56 + HCN. We looked for a possible concerted decomposition pathway for this. Instead, we find a stepwise mechanism via the formation and decomposition of INT130. The barrier for the formation of INT130 at TS7 is 45.0 kcal/mol. The formation of INT130 occurs by the elimination of an HCN molecule from INT157 through a ring-breaking mechanism. INT130 was also observed as an intermediate in our earlier RDX decomposition mechanism, which upon further decomposition leads to MN and INT56. INT130 formed here is a ring-opened structure of INT130 formed in the RDX decomposition mechanism. The ring-opened INT130 is a very unstable intermediate and requires only 2.5 kcal/mol to decompose to MN and INT56. The decomposition transition state TS8 has the breaking CN bond at 1.839 Å. The final products are 48.9 kcal/mol more endothermic than HMX.

5.3.5. Summary of N−N Homolysis Pathway Calculations. Four different product channels have been identified for the N−N homolysis pathway (Figure 4). Two of these channels, degradation of HMX to RDR-o and INT222, relate the decomposition mechanism of HMX to RDX.

5.4. Reaction Pathway 2: Concerted HONO Elimination. The most exothermic reaction pathway found in our earlier RDX decomposition mechanism was the consecutive HONO elimination leading to 3HONO + 3HCN.[18] We searched for similar pathway in the HMX decomposition.

Due to the weak equatorial N−N bond and close nonbonded CH::O contact, HONO elimination can occur by preferential elimination of equatorial NO_2 in HMX. TS9 is the transition structure for first HONO elimination and has a barrier of 44.6 kcal/mol over HMX. Thus, the initiation of HONO elimination requires an additional 5.6 kcal/mol over N−N homolytic cleavage. The structure of TS9 is very similar to the HONO elimination TS found in RDX and other related compounds: dimethynitramine[35] and MN.[33,36] The breaking N−N bond is 2.058 Å and the forming CN π and OH σ bonds are 1.342 and 1.248 Å. The HONO elimination barrier in HMX is 4.8 kcal/mol higher than in RDX. HONO elimination leads to INT249, which is 4.0 kcal/mol endothermic than HMX (Figure 5).

5.4.1. Second and Third HONO Elimination. INT249 can eliminate a molecule of HONO via TS10 to form INT202, leading to TS10 with energy 45.0 kcal/mol above HMX. INT202

can subsequently eliminate another molecule of HONO via TS11. TS11 has a barrier of 36.0 kcal/mol over HMX, leading to a stable intermediate INT155. The successive HONO elimination sites from INT249 and INT202 were chosen based on the closest nonbonded O:::H contacts. INT202 and INT155 are respectively 2.5 and 12.9 kcal/mol more exothermic than HMX.

5.4.2. Fourth HONO Elimination. INT155 can subsequently eliminate another HONO molecule via TS12 to form a stable intermediate (INT108). TS12 is 28.3 kcal/mol above HMX. The decomposition of HMX to 4 HONO + INT108 is exothermic by 19.3 kcal/mol. Of the various unimolecular decompositions from HMX, this is the most exothermic (energy released) pathway found in the present study. This is also in agreement with our earlier RDX decomposition study.[18]

In TS12 the breaking N−N bond is 2.131 Å and the C−H bond is 1.317 Å whereas the forming OH bond is 1.332 Å and the CN π bond is 1.346 Å, respectively. The CN π bonds in INT108 are localized due to its nonplanar conformation. Thus, there are two distinct sets of C−N bonds of double (1.283 Å) and single (1.383 Å) character.

5.4.3. INT108 Concerted Decomposition. INT108 is a stable intermediate and it decomposes through a concerted mechanism to four HCN through an energy barrier of 106.7 kcal/mol (TS13) located by simultaneously scanning all the four CN σ bonds. We did not put any symmetry restriction to locate TS13. Considering that INT108 + 4HONO is 19.3 kcal/mol more exothermic than HMX, the overall energy required for the decomposition is 87.4 kcal/mol with respect to HMX. The final products, 4HCN + 4HONO are 18.9 kcal/mol endothermic from HMX.

TS13 is a nonplanar TS with the breaking CN bonds at ∼1.9 Å, while the fragment HCN molecules are each close to the final product linear structure (H−C−N angles ∼144°).

5.5. Reaction Pathway 3: CH_2O + N_2O Formation. Formation of CH_2O and N_2O has been extensively considered as the major decomposition products in the thermal decomposition of HMX.[2−17] However, there is no conclusive experimental identification of the source of these molecules. Two possible mechanisms has been proposed:

(i) direct decomposition of HMX via oxygen migration and subsequent decomposition, and

(ii) secondary decomposition from MN.

To understand the mechanism of CH_2O and N_2O formation, we examined the former mechanism.

To locate the transition state of oxygen migration, we scanned one of the nonbonded C···O distance in HMX. As the oxygen atom of NO_2 group approaches the C atom, the HMX ring opens up via the breaking of the neighboring CN bond, leading to a ring-opened INT296 intermediate (Figures 2 and 6). The oxygen migration generally leads to a oxy-ring type structure, which can undergo further decomposition to smaller products. The 10-member cyclic oxy-ring molecule might not be stable in the case of HMX and instead the neighboring CN bond breaks in TS14 to form an acyclic biradical intermediate INT296. TS14 has a barrier of 55.3 kcal/mol over HMX. The forming C−O bond is 1.624 Å and the breaking CN bond is 2.293 Å in TS14. INT296 is a ring-opened structure with one end having a four-member oxy-ring and the other end the N−NO_2 radical. The radical center in N−NO_2 is delocalized toward the O atom. The larger N−O bond (1.22−1.27 Å) and shorter N−N bond (1.40−1.33 Å) is evidence for this. The structure and energy of INT296 are very close to the TS14 and only 0.3 kcal/mol more stable than TS14 without ZPE correction. With ZPE correction the energies of TS14 and INT296 are very close, but optimization along the reaction coordinate of the imaginary frequency in TS14 leads to INT296. INT296 can further decompose to INT222 and the four-membered oxy-ring (−$OCH_2NN(O)$−, MN-oring) structure. Scanning the CN bond reveals that the formation of INT222 + MN-oring is a barrier less process from INT296 with an overall endothermicity of 80.3 kcal/mol with respect to HMX. INT222 has the same ring-opened RDX structure found in the N−N homolysis pathway.

MN-oring is the stable intermediate formed in the oxygen migration pathway of MN to form CH_2O and N_2O. This has also been identified as a stable intermediate in MN decomposition mechanism.[33] Decomposition of MN-oring to CH_2O + N_2O requires 25.3 kcal/mol. This is in good agreement with the G2M calculated energy barrier of 25.8 kcal/mol.[33]

5.5.1. Formation of CH_2O + N_2O from RDX. As mentioned above, CH_2O and N_2O can be formed directly from RDX or HMX by an oxygen transfer mechanism in addition to the much considered MN decomposition pathway. We examined this an additional decomposition pathway of RDX after our earlier work.[18]

To locate the transition structure of oxygen migration, we scan one of the nonbonded C···O distances similar to HMX. As the oxygen atom of the NO_2 group approaches the C atom of the CH_2, the CN bond between the N atom (containing the NO_2 group) and the C atom breaks to form an eight-member oxy-ring intermediate (RDX-oring). As mentioned earlier, this results in a ring-opened intermediate in HMX, instead of forming a similar 10 member oxy-ring structure. The RDX-oring formed via the O-atom migration is quite stable intermediate and has 14.0 kcal/mol more energy than RDX (Figure 6b). The transition structure for O migration TS15 has a barrier of 52.7 kcal/mol over RDX. This is quite high compared to the other two initial decomposition processes in RDX: N−N homolysis 39.0 kcal/mol and HONO elimination 39.2 kcal/mol. TS15 has a very loose structure. The breaking C−N and N−O π bonds are 2.333 and 1.272 Å, and the forming C−O and N−N π bonds are 2.346 and 1.335 Å. Transits in the forward and backward directions along the imaginary frequency reaction coordinate confirm that TS15 properly connects RDX with RDX-oring.

The N−O, C−O, and N−N bonds are 1.545, 1.401, and 1.248 Å, respectively, in RDX-oring. The structure of RDX-oring is shown in Figure 2. RDX-oring can further dissociate to CH_2O + N_2O + 2MN in a concerted manner via TS16. The barrier for this concerted breaking is 24.2 kcal/mol. The structure of TS16 is shown in Figure 3. The final products are 10.5 kcal/mol endothermic than RDX. The N_2O fragment in TS16 is quite close to its isolated structure and the breaking C−N and N−O bonds are 2.026 and 2.233 Å. The dissociating CH_2O fragment has an intermediate character with the breaking C−N bond at 1.592 Å, only 0.13 Å longer than the C−N bond in RDX. The C−O bond in the CH_2O fragment is 1.321 Å, between a double and single bond character. The other two MN fragments are still connected with the dissociating C−N bond at 1.513 Å, but will undergo dissociation along the reaction coordinate to form two MN fragments.

5.5.2. Summary of o-Migration Calculations. Additional pathways for the formation of CH_2O and N_2O directly from RDX and HMX have been identified. Associated large endothermicity suggests that CH_2O and N_2O formation preferably occur through the secondary decomposition of MN for HMX. In contrast, the direct oxygen migration pathway is an important reaction channel for the formation of CH_2O and N_2O in RDX.

6. Discussion

The commonality between the HMX and RDX decomposition pathways led us to propose a unified mechanism. This is pictorially presented in Figure 7. Majority of the decomposition products observed experimentally can be accounted for by the present scheme. It should be noted that the present work and our earlier paper[18] study gas phase kinetics. There is some correlation of gas phase mechanisms with condensed phase experimental results. Furthermore, the present scheme cannot explain some of the mass fragments resulting from bimolecular reactions such as ONTNTA or ONDNTA observed by Behrens and Bulusu[10,37] in the thermal decomposition of RDX and HMX.

6.1. Identification of Mass Fragments with $M \geq 100$. HMX pyrolysis is a complex phenomena involving nonlinear processes as demonstrated by the temporal dependence of the thermally decomposed products.[10−12] Most recent experiments on HMX[10−12,14,15] detected mass fragments of $m/z \leq 100$ as the major thermal decomposition products. Behrens has argued that the higher molecular weight fragments detected in some earlier experiments, such as flow reactor mass spectrometry (FRMS) and solid probe mass spectrometry (SPMS) and those using appearance energy measurements,[3,4] could not be unambiguously considered as thermal decomposition products. These higher molecular weight fragments could have originated from ion fragmentation of HMX vapor (second channel below):

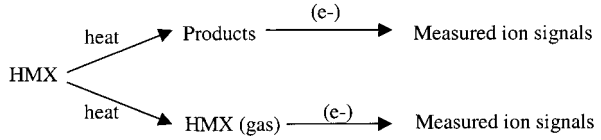

In these experiments, HMX is heated in a vacuum environment and then electron bombardment is used to ionize and subsequently measure the mass fragments. These higher molecular weight species are similar to those detected in the mass spectrum of HMX.[2b] Therefore, in our discussions, the calculated high molecular weight mass fragments are compared primarily with the mass spectroscopic data[2b] and with earlier thermal decomposition data[3,4] where appropriate. Within the scope of the present ab initio study we cannot characterize the ion fragmentation process of HMX, which requires cross sections for electron bombardment reactions.

Our present scheme can explain the following mass fragments with $m/e \geq 100$: 296, 250, 249, 222, 204, 202, 176, 175, 158, 157, 155, 149, 130, 128, 108, and 102. Many of these fragments are from the short-lived intermediates, which undergo further decomposition instantaneously and hence might not be observed experimentally. Ions of m/z values of 75, 120, 128, 148, and 222 are the major ions observed in the mass spectrum of HMX.[2b] On the other hand, larger mass fragments detected experimentally in the thermal pyrolysis are 280, 250, 249, 222, 206, 176, 175, 148, 132, 128, 120, and 102. However, Zhao et al. detected only two of these larger mass fragments at 120 and 102 in their laser photolysis of the RDX molecular beam.[1] Masses at $m/e = 280$ (ONTNTA) and 206 (ONDNTA) were detected by Behrens and Bulusu in the thermal pyrolysis of HMX and RDX.[10,37] These nitroso compounds were considered as resulting from removal of a NO_2 group followed by association of NO radical at the N-radical center of RDX or HMX. Such bimolecular formations of nitroso compounds have not been addressed in our unimolecular decomposition scheme.

Mass fragments of 250 and 176 are HMR and RDR radical generated after removal of NO_2 radical from HMX and RDX, respectively. These radicals have been identified in the condensed phase decomposition of RDX and HMX.[4,8,9] Zhao et al. did not observe $m/e = 176$ in their IRMPD study.[1] Presence of excess energy in the laser pulse might cause further decomposition of this to smaller mass fragments. Mass fragments 249 and 175 result from elimination of the first HONO molecule from HMX and RDX. The computed HONO elimination pathway for RDX and HMX suggest that these mass fragments would not be very stable and should undergo further dissociation to smaller more stable species. Furthermore, the mass peak at 128 is assigned to the structure resulting from the second HONO elimination in RDX. Goshgarian[3] and Fifer[9] observed the mass peak at 128 resulting from HONO elimination from RDX and from the HMX fragments at $M = 222$. Similar structure for mass fragment $M = 128$ was postulated in the mass spectra of RDX and HMX.[2b] Stability of these radicals in the condensed phase might be responsible for their detection. However, Zhao et al. did not detect larger mass fragments of 175 and 128 in their laser photolysis of RDX molecular beam.[1]

Formation of mass fragments at $m/e = 222$ was found in N−N homolysis and O-migration pathways of HMX decomposition. This INT222, formed by the removal of CH_2N radical from HMR-o (Figure 4), or by the removal of MN-oring from INT296 (Figure 6a), has a ring-opened RDX structure. This could be cyclized to RDX as shown by the double arrow in Figure 7. Bulusu et al. observed an ion peak at m/z 222 in the mass spectrum of HMX.[2b] Goshgarian[3] and Fifer[9] also observed this mass peak in the thermal decomposition of HMX. However, no definitive conclusion was reached as to whether the structure corresponds to RDX or its ring opened form.

Although $m/e = 120$ was detected by Zhao et al.[1] in the gas phase laser photolysis, in our RDX ab initio calculations we did not find a primary decomposition pathway for its formation. To account for $m/e = 148$, 120 in the mass spectra of HMX, Bulusu et al. considered migration of a CH_2 hydrogen to the neighboring NO_2 followed by ring contraction as the initiation mechanism.[2b] They also proposed a HONO group migration in the formation of the ion at m/z 120. Our calculations clearly indicate that such migration will preferably lead to the exothermic HONO elimination. Alternatively, in an earlier thermal decomposition study,[4] Farber and Srivastava suggested that the peak at m/z 120 might come from the reactions of gaseous products with the condensed phase. Bimolecular association of the MN molecule with the NO_2 radical could fit this postulate. Farber and Srivastava proposed a homolytic cleavage of the HMX ring to two $CH_2N(NO_2)CH_2NNO_2$ biradicals, which can further undergo cyclization to a four-membered ring. We tried to scan this homolytic cleavage of HMX to generate radical 148. We did not find any converged structure for this because optimization of this radical always resulted in decomposition to two MN molecules. Our present scheme cannot account for these experimentally observed mass fragments. The mass peak at 102 results from the elimination of one MN molecule from RDR-o and can come from the decomposition of both RDX and HMX as shown in Figure 7. This peak was observed in condensed phase decomposition,[4,8,9] *in mass spectra*,[2b] as well as in the gas phase study.[1]

The mass fragment at 108 is the result of successive 4HONO elimination from HMX, as shown in Figure 7. This mass peak was not detected experimentally. On the other hand, decomposition of HMX to 4HCN + 4HONO is considered to be one of the most important condensed phase processes.[17] Figure 5 shows that decomposition of HMX to 4HCN and 4HONO must occur via the formation of INT108. In our calculations, INT108 was found to be the most exothermic decomposition product from

HMX, like the formation of TAZ (81) from RDX. The available energy in most of these experiments might be sufficient to overcome the decomposition barrier of INT108 (87.4 kcal/mol with respect to HMX). Further gas phase experiments with precisely tuned laser energy might provide more insight.

6.2. Identification of Mass Fragments with $46 \leq M \leq 100$. The mass fragments in this range that can be explained by our present scheme are 81, 75, 74, 56, 47, and 46. Experimentally observed mass fragments in this range are 97, 81, 75, 74, 70, 59, 56, 54, 47, and 46.

Mass fragments at 46 and 47 were found in the N−N homolysis and HONO elimination pathways of RDX and HMX decomposition. These mass peaks are unambiguously identified as NO_2 and HONO in most of the experiments. However, the stability of HONO is questionable and its further decomposition to OH and NO may be responsible for its absence in some experiments.[1,17] We computed a barrier of 49.6 kcal/mol for the latter process. Both 46 and 47 mass fragments could as well result from the decomposition of MN (74).

MN (74) was observed as one of the major products in almost all these reaction pathways. Concerted decomposition of RDX to three MN molecules, which requires 59.4 kcal/mol, was identified as the most important decomposition pathway for RDX by Zhao et al.[1] We could not find a similar transition state for HMX decomposition to four MN molecules. Thus, the MN fragments found in HMX decomposition must come from the other three decomposition channels, presented in Figures 4, 5, and 6. In addition, MN-oring found in the HMX O-migration pathway (Figures 6a and 7) has the same molecular mass of 74. MN-oring could well be generated via a similar O-migration mechanism from MN.[33] Behrens and Bulusu[11] observed a $m/e = 74$ for $C_2H_6N_2O$ in their thermal pyrolysis of HMX. This was assigned to $(CH_3)_2NNO$. We believe that this species results from the bimolecular association of decomposition products and hence is not present in our scheme.

The mass peak at $m/e = 75$ is MNH formed from the decomposition of RDR-o as shown in Figure 7. Goshgarian observed this species in the thermal decomposition of RDX and HMX and considered MNH as one possible candidate.[3]

Mass fragment 56 was identified in laser pyrolysis[38] and photolysis[1] experiments and the chemical structure is CH_2N-CHNH. It can result from the N−N homolysis pathway in both RDX and HMX. As shown in Figure 4, a low-energy pathway for HMX involves elimination of two NO_2 radicals, followed by sequential elimination of HONO, HCN, and MN to form INT56.

The mass peak at 81 can be identified as TAZ, observed in most condensed phase experiments and also in the gas phase photolysis of RDX. This results from successive elimination of three HONO molecules from RDX and is the most exothermic pathway in our mechanism.[18] TAZ cannot be formed directly from HMX except via the formation of RDX. Goshgarian[3] and Fifer[9] proposed the formation of TAZ from HMX via the formation and decomposition of species with m/e 222. This could as well be RDX or its ring open form (INT222), as shown in Figure 7. Behrens and Bulusu[39] made no mention of this species in liquid phase HMX decomposition, but Behrens[11] observed this in electron ionization of HMX. Recently, Tang et al. concluded from their CO_2 laser assisted combustion of HMX that the peak at mass 81 could not be from the fragments of HMX in the ionizer.[14]

Masses 97 and 70 were postulated to have chemical formulas $C_3N_3H_3O$ and $C_2N_2H_2O$, while their chemical structures remain uncertain. Oxy-*s*-triazine (OST) was considered as the most plausible candidate for $C_3N_3H_3O$.[14,37,38] Behrens and Bulusu[37] identified OST as the only unimolecular product in RDX decomposition. They also proposed a plausible mechanism for its formation and concluded that HONO elimination is the rate-controlling step. Tang et al. found a small amount of this species in their laser pyrolysis experiment.[14] As mentioned in our earlier work on RDX,[18] OST formation occurs preferably from INT128 (generated after 2 HONO elimination from RDX) but does not follow the Behrens and Bulusu mechanism. Nitro−nitrite rearrangement followed by HNO elimination (which has a 54.5 kcal/mol barrier with respect to RDX) or by O-migration from NO_2 to neighboring C-atom followed by rearrangement and HNO elimination (barrier of 64.8 kcal/mol with respect to RDX) from INT128 could be other possibilities. However, none of these mechanisms can justify HONO elimination as the rate-limiting step. 70 was assigned as a daughter ion formed from OST.[37] Lee et al. identified 70 as a true decomposition product from RDX.[38] We believe a possible formation route of 70 would follow the sequential elimination of HCN from OST.

Mass 54 was observed in the laser pyrolysis of RDX and HMX as a decomposition product of TAZ.[14,38] This is only possible via a sequential elimination of HCN from TAZ. We believe that concerted decomposition of TAZ to 3HCN will be more favorable energetically. On the other hand, mass 59 was assigned to *N*-methylformamide (CH_3NHCOH) by Behrens and Bulusu.[10] They suggested that such amide products are formed by bimolecular association of initial decomposition fragments or by the decomposition of the nonvolatile polyamide observed in their experiment.

In their analytical pyrolysis-atmospheric pressure ionization (PY-API) tandem mass spectrometry study of HMX, Snyder et al.[40] identified mass peaks at m/z values 44, 46, 60, 74, 75, 85, 98, 30, 58, 69, 71, 83, and 141. The first seven ions were considered common to RDX and HMX decompositions. Moreover, isotope scrambling experiments revealed that except for the ion at m/z 75, nitrogen atoms of all other observed ions are derived from the ring rather than the nitro group. Thus, the observed chemical species in this experiment is very different from the other experiments. They argued that the effects due to vaporization and ionization/fragmentation of undecomposed reactants were minimized or avoided by carrying out the pyrolysis at atmospheric pressure. Behrens also observed some of these mass fragments as true pyrolysis product.[10−12] Such products might as well originate from intermolecular reactions among the decomposed products, especially at high pressures, and not be true unimolecular decomposition products. A majority of the thermal decomposition experiments on RDX and HMX observed some mass fragments, which could be only explained as originating from bimolecular reactions. Theoretical studies of these interactions require molecular dynamics of RDX and HMX crystals with a force field capable of treating molecular reaction. Such an effort has been initiated at our center.[41]

6.3. Gas Phase Chemistry. Smaller mass fragments from unimolecular decomposition lead to gaseous products via further reaction. Experimentally observed small mass fragments such as 46 (NO_2), 44 (N_2O), 30 (NO, CH_2O), 28 (CH_2N), 27 (HCN), 17 (OH) can be explained based on our scheme presented in Figure 7. Other small mass fragments detected experimentally such as 45 (formamide),[14,37] 43 (HNCO),[14] or 42 (C_2H_4N)[14] might not be true decomposition products of RDX and HMX. Many of the smaller mass fragments such as CO, CO_2, H_2O, N_2, H_2 etc. results from bimolecular reactions such as

$$CH_2O + N_2O \rightarrow H_2O + CO + NO$$

Reactions among these unique unimolecular decomposition species define the different zones in the flame structure of RDX and HMX combustion. The gas phase chemistry of nitramine combustion has been modeled recently.[42]

7. Concluding Remarks

From our mechanistic studies in the gas phase we conclude the following:

(i) Consecutive HONO eliminations (leading to TAZ + 3HONO from RDX and INT108 + 4HONO from HMX) are energetically the most favorable pathways. Further decomposition of TAZ to 3HCN and INT108 to 4HCN requires relatively higher energy. However, decomposition of RDX and HMX to HCN and HONO (and OH + NO on further decomposition) is considered one of the most important global reactions for nitramines, both from experimental[7] and theoretical[23] point of view.

(ii) Formation of CH_2O and N_2O can occur from RDX either by O-migration followed by concerted decomposition of the stable RDX-oring intermediate or by secondary decomposition of MN. The former is energetically more favorable and is one of the most important decomposition channels for RDX in addition to HONO elimination. In contrast CH_2O and N_2O formation in HMX occurs preferably from MN secondary decomposition.

(iii) Concerted decomposition of RDX to three MN molecules is another important pathway. Decomposition of RDX through this pathway requires higher energy than the other two, which is at variance with the inferred results from gas phase experiments. We did not find a similar pathway for HMX.

(iv) The N−N bond cleavage to form RDR from RDX or HMR from HMX is another favorable pathway but the associated endothermicity for further dissociation makes this channel less favorable. However, the N−N homolysis pathway unifies RDX and HMX mechanisms and can explain many of the common mass fragments observed experimentally.

(v) The unified scheme successfully accounts for majority of the mass fragments observed in the thermal decomposition of RDX and HMX. It does not include catalytic decomposition pathways or bimolecular reactions in condensed phase.

(vi) Predicted energetics of the RDX decomposition give good qualitative agreement with results of the gas phase molecular beam experiments. Similar gas phase experiments in HMX will allow more rigorous comparisons with experiments.

Acknowledgment. This research was supported by the Caltech DoE -ASCI-ASAP project. The MSC facilities are also supported by grants from NSF CHE (95-12279), Chevron Corp., ARO-MURI, Beckman Institute, Exxon, Owens-Corning, Avery-Dennison, Dow Chemical, 3M, NIH, Asahi Chemical, BP Amoco, and ARO ASSERT.

Supporting Information Available: Optimized geometry of the intermediates and some important products and transition states. This material is available free of charge via the Internet at http://pubs.acs.org.

References and Notes

(1) Zhao, X.; Hintsa, E. J.; Lee, Y. T. *J. Chem. Phys.* **1988**, *88*, 801.
(2) (a) Suryanarayana, B.; Graybush, R. J.; Autera, J. R. *Chem. Ind., London*, **1967**, *52*, 2177. (b) Bulusu, S.; Axenrod, T.; Milne, G. W. A. *Org. Mass. Spectrom*. **1970**, *3*, 13.
(3) Goshgarian, B. B. *AFPRL-TR-78-76* Oct **1978**.
(4) Farber, M.; Srivastava, R. D. *Proc. 16th JANNAF Combust. Meeting*; CPIA Publ. 308 **1979**, *2*, 59.
(5) Morgan, C. V.; Bayer, R. A. *Combust. Flame* **1979**, *36*, 99.
(6) Oxley, J. C.; Kooh, A. B.; Szekers, R.; Zhang, W. *J. Phys. Chem.* **1994**, *98*, 7004.
(7) Flanigan, D. A.; Stokes, B. B. *AFRPL-TR-79-94* Oct **1980**.
(8) Schroeder, M. *Proc. 16th JANNAF Combust. Meeting*; CPIA Publ. 308; **1979**, *2*, 17.
(9) Fifer, R. A. In *Fundamentals of Solid Propellant Combustion, Progress in Astronautics and Aeronautics*; Kuo, K. K., Summerfield, M., Eds.; AIAA Inc.: New York, 1984; Vol. 90, p 177.
(10) Behrens, R., Jr.; Bulusu, S. *J. Phys. Chem*. **1991**, *95*, 5838.
(11) Behrens, R., Jr. *Int. J. Chem. Kinet*. **1990**, *22*, 135.
(12) Behrens, R., Jr. *J. Phys. Chem*. **1990**, *94*, 6706.
(13) Boggs, T. L. In *Fundamentals of Solid* Propellant *Combustion, Progress in Astronautics and Aeronautics*; Kuo, K. K., Summerfield, M., Eds.; AIAA Inc.: New York, 1984; Vol. 90, p 121.
(14) Tang, C.-J.; Lee, Y. J.; Kudva, G.; Litzinger, T. A. *Combust. Flame* **1999**, *117*, 170.
(15) Tang, C.-J.; Lee, Y. J.; Litzinger, T. A. *J. Prop. Power* **1999**, *15*, 296.
(16) Korobeinichev, O. P.; Kuibida, L. V.; Madirbaev, V. *Zh. Fiz. Goreniya I Vzryva* **1984**, *20*, 43.
(17) Brill, T. B. *J. Prop. Power* **1995**, *11*, 740.
(18) Chakraborty, D.; Muller, R. P.; Dasgupta, S.; Goddard, W. A., III *J. Phys. Chem. A* **2000**, *104*, 2261.
(19) Smith, G. D.; Bharadwaj, R. K. *J. Phys. Chem. B* **1999**, *103*, 3570.
(20) Sorescu, D. C.; Rice, B. M.; Thompson, D. L. *J. Phys. Chem. B* **1998**, *102*, 6692.
(21) Sorescu, D. C.; Rice, B. M.; Thompson, D. L. *J. Phys. Chem. B* **1999**, *103*, 6783.
(22) Pati, R.; Sahoo, N.; Das, T. P. *J. Phys. Chem. A* **1997**, *101*, 8302.
(23) (a) Melius, C. F.; Binkley, J. S. *Symp. (Int.) Combust., [Proc.], 21st* **1986**, 1953. (b) Melius, C. F. In *Chemistry and Physics of Energetic Materials*; Bulusu, S. N., Ed.; Kluwer: Dordrecht, 1990; p 21.
(24) Becke, A. D. *J. Chem. Phys*. **1993**, *98*, 5648, 1372; **1992**, *96*, 2155; **1992**, *97*, 9173.
(25) Lee, C.; Yang, W.; Parr, R. G. *Phys. Rev.* B **1988**, *37*, 785.
(26) Wu, C. J.; Fried, L. E. *J. Phys. Chem. A* **1997**, *101*, 8675.
(27) Harris, N. J.; Lammertsma, K. *J. Am. Chem. Soc*. **1997**, *119*, 6583.
(28) (a) Jaguar 3.5; Schrödinger Inc.: Portland, OR, 1998. (b) Greeley, B. H.; Russo, T. V.; Mainz, D. T.; Friesner, R. A.; Langlois, J.-M.; Goddard, W. A., III; Donnelly, M. N.; Ringnalda, R. E. *J. Chem. Phys*. **1994**, *101*, 4028.
(29) Choi, C. S.; Boutin, H. P. *Acta Crystallogr*. **1970**, *B26*, 1235.
(30) Cady, H, H,; Larson, A. C.; Cromer, D. T. *Acta Crystallogr*. **1963**, *16*, 617.
(31) Main, P.; Cobbledick, R. E.; Small, R. W. H. *Acta Crystallogr*. **1985**, *C41*, 1351.
(32) Cobbledick, R. E.; Small, R. W. H. *Acta Crystallogr*. **1974**, *B30*, 1918.
(33) Chakraborty, D.; Lin, M. C. In *Solid Propellant Chemistry, Combustion, Progress in Astronautics and Aeronautics and Motor Interior Ballistics*; Yang, V., Brill, T. B., Ren, W.-Z., Eds.; 2000; Vol. 185, p 33.
(34) Harris, N. J.; Lammertsma, K. *J. Am. Chem. Soc*. **1996**, *118*, 8048.
(35) Harris, N. J.; Lammertsma, K. *J. Phys. Chem. A* **1997**, *101*, 1370.
(36) Rice, B. M.; Adams, G. F.; Page, M.; Thompson, D. *J.* Chem. *Phys.* **1995**, *99*, 5016.
(37) Behrens, R., Jr.; Bulusu, S. *J. Phys. Chem*. **1992**, *96*, 8877, 8892.
(38) Lee, Y.; Tang, C.-J.; Litzinger, T. A. *Combust. Flame* **1999**, *117*, 600.
(39) Behrens, R., Jr.; Bulusu, S. *Mater. Res. Soc. Symp. Proc*. **1993**, *296*, 13.
(40) Snyder, A. P.; Liebman, S. A.; Bulusu, S.; Schroeder, M. A.; Fifer, R. A. *Org. Mass. Spectrom.* **1991**, *26*, 1109.
(41) Van Duin, A. C. T.; Dasgupta, S.; Goddard, W. A., III, manuscript in preparation.
(42) Yetter, R. A.; Dryer, F. L.; Allen, M. T.; Gatto, J. L. *J. Prop. Power* **1995**, *11*, 683.